Turkish Journal of Electrical Engineering & Computer Sciences

http://journals.tubitak.gov.tr/elektrik/

Research Article

Turk J Elec Eng & Comp Sci
(2017) 25: 1693 – 1711

doi:10.3906/elk-1502-118

Loss minimization in wind farm integrated AC/DC system by optimal injections and droop settings of VSC-MTDC systems

Anbuselvi SHANMUGAM VELU*, Somasundaram PERIYASAMY, Kumudini Devi RAGURU PANDU
College of Engineering Guindy, Anna University, Chennai, India

Received: 15.02.2015 • **Accepted/Published Online:** 11.06.2016 • **Final Version:** 29.05.2017

Abstract: In this paper, a modified optimal power flow (OPF) model, incorporating a voltage source converter-based multiterminal DC (VSC-MTDC) system, is proposed. The OPF is formulated to minimize the losses, steady state voltage deviations, and overloading of the AC/DC system. The control variables considered in this modified OPF model are power injection into the DC system and droop settings. Optimal injection patterns for different wind power penetrations and optimal droop settings are evaluated for wind farm side converters and grid side converters, respectively. Wind power penetrations are routed into AC and DC lines in different proportions to optimize the flows in AC/DC lines. The VSC-MTDC system, embedded on a practical utility system, is considered for the analysis. The results reveal that the losses are significantly reduced and flows in the AC and DC networks are optimally controlled to maximize the evacuation capability of the AC/DC system.

Key words: Voltage source converter-based multiterminal DC optimal power flow, droop control, optimal injections, loss minimization

1. Introduction

Voltage source converter-based MTDC (VSC-MTDC) has gained widespread attention in industry and academia [1]. VSC two-terminal HVDC projects have emerged worldwide and the relevant technology has attained maturity. The VSC-HVDC link is a most viable solution for integrating wind power into the grid [2,3], due to its capability to operate with a low short-circuit ratio (SCR). Mostly wind power is integrated into the power system at subtransmission level. The SCR at the PCC is normally low and is bound to undergo changes when the system topology changes. VSC-MTDC links offer the advantage of independently controlling real and reactive power in all four quadrants, irrespective of the SCR [4]. The smaller footprint and ease of erecting new DC substations within very small spans of time helps to keep in phase with new capacity additions. Meshed AC/DC supergrids [5] are likely to appear in the near future to provide a more reliable, greener smart grid.

Droop control is a standard technique adopted in the control of VSC-MTDC systems. The effect of droop settings on steady state power flow within the DC grid, and in the AC system connected to the DC grid, can be analyzed by using load flow analysis with droop implementation [6,7]. It is an extension of conventional VSC-MTDC load flow analysis [8] with a distributed slack bus. Basically, there are two variations of droop control reported in the literature [7]. The difference between the behavior of V-P droop and V-I droop is almost

*Correspondence: svanbuselvi@annauniv.edu

negligible. The effect of droop control action is shown to be the power-sharing within the DC grid by regulation of the DC voltages. The DC bus voltage regulation is distributed among the droop-controlled buses in the DC grid [9–11]. The effects of voltage limits and dead bands on droop characteristics are analyzed with respect to the power-sharing of the converter.

Many authors focus on minimizing the cost of VSC-MTDC projects [12–15] by minimizing loss. The problem is conventionally viewed as a planning problem. Various parameters, such as cable-laying cost, cable cost, converter costs, offshore converter platform cost, and DC protection cost, were optimized. Extended AC/DC OPF, for evaluating different MTDC alternative topologies to maximize cost benefits, were considered in [14]. Various MTDC topologies such as series, ring, and radial were considered, as shown in Figure 1. Cost benefits were evaluated over a period of time for different DC subsystem topologies. Total economic benefits due to reduction of generation cost and reduction of losses were evaluated. Grid code compliance [15] is also included in the OPF formulation by including the constraints on voltage and power factor at the point of common coupling (PCC). An optimal trade-off should be made between power-sharing and maximum allowable DC voltage deviation following an outage [16].

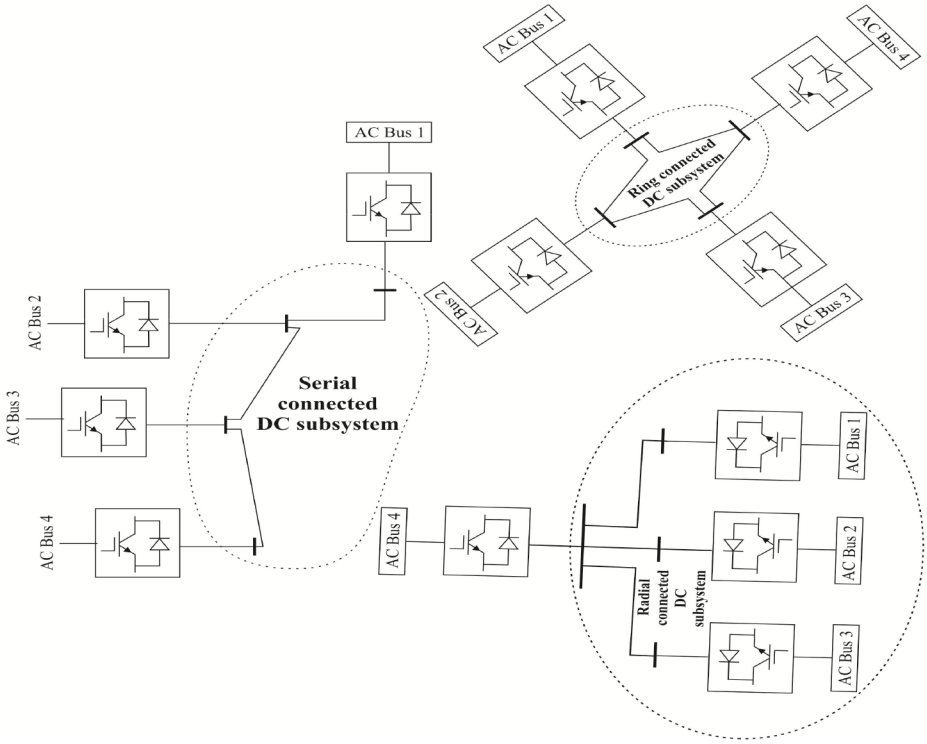

Figure 1. Serial, radial, and ring topology of the VSC-MTDC system.

Optimizing the droop settings at the grid side converter (GSC) and power injections at the wind farm side converter (WFSC) for a preoptimized AC/DC network topology still needs to be addressed. Implementation of droop control at GSCs and injection control in WSCs to minimize losses, voltage deviations, and overloading of the AC/DC system is not discussed in the literature to the best of our knowledge. Optimizing the loading in the AC/DC network at the cost of slight increase in losses gains importance in high wind season, especially when the grid frequency needs to be increased. Backing down wind power due to congestion in transmission corridors is one of the issues that needs to be addressed in South India.

The main objective of this paper is to propose an OPF model to minimize system operational losses, steady state voltage deviations, and overloading of the AC/DC system by optimizing injection into the DC subsystem at the WFSC and droop settings at the GSC in a VSC-MTDC link embedded in the AC system. As a preoptimization problem, the topology of the DC subsystem is chosen based on rigorous cost/benefit analysis [14]. The VSC-MTDC system considered is meant for network reinforcement of an AC transmission system, evacuating wind power. As the wind power fluctuates, the flows in the AC lines and the DC links are regulated by appropriate injections into the DC grid at various rectifier buses and droop settings for the inverter buses. Thus, the problem is posed as an operational problem, rather than as a planning problem.

2. Control of the MTDC system

VSC-MTDC controllers can control both real and reactive power in a decoupled manner. In a two-terminal system, the DC voltage and the AC bus voltage/reactive power are the control parameters of the DC slack bus. The other bus regulates the real and reactive power injection into the two-terminal DC link. The DC slack bus power is unknown prior to load flow. This stems from the fact that if the power injection into the DC system is fixed the power drawn from the inverter side is an unknown parameter, since losses cannot be computed prior to load flow analysis. Conventionally independent PQ/PV control is adopted through grid voltage vector orientation control. The current control references are given by the outer controllers [17]. The fast inner controllers track the current references by dynamically controlling the d and q axis voltages at the converter AC buses.

In the case of multiterminal systems, power pooled into the DC grid through various rectifier buses is pumped at different inverter buses. Unlike two-terminal systems, where a slack bus holds the responsibility of maintaining the DC link voltage and power balance, distributed control of system voltage is adapted to improve robustness. The responsibility of regulating DC voltage is shared by a number of controllers operating in droop control mode. Contrary to the case with one slack bus, the power set points of all the droop-controlled buses are modulated to maintain the power balance in the system. The droop controller is the outermost controller with a larger time constant when compared to the cascaded controller, as shown in Figure 2. The buses in the DC link are classified as droop-controlled buses and P-controlled buses. The P-controlled buses are taken to be those DC buses connected to wind farms, and droop-controlled buses are taken to be those DC buses from where the power pooled into the DC link is evacuated into the upstream transmission system. The power order of the P-controlled bus is optimally set by the operator based on wind power penetration, converter outages, rating of DC link converters, and congestion in the AC line.

The slow centralized coordinated controller (SCCC) regulates the power-sharing among the converters by regulating the droop settings. The power order of the droop-controlled bus is modulated around the reference set by the SCCC by the droop controller. The share of power evacuated through the inverter buses in the system is regulated by droop control. The droop constant is normally stated as a change in the DC grid power flow in MW as a result of 1 kV change in DC voltage [11]. It is worth mentioning that without droop control, the DC slack bus or the overrated inverter DC bus serves to ensure the voltage regulation and power-balancing in the DC system.

DC voltages and power order settings at various converters are the essential parameters dictating the flows within the MTDC system. The SCCC is the outermost controller, regulating the droop settings of GSCs and the power injection set points of WFSCs in this study. Wind power penetrations can be routed into AC and DC lines in different proportions. These proportions could be determined by optimizing the flows in various

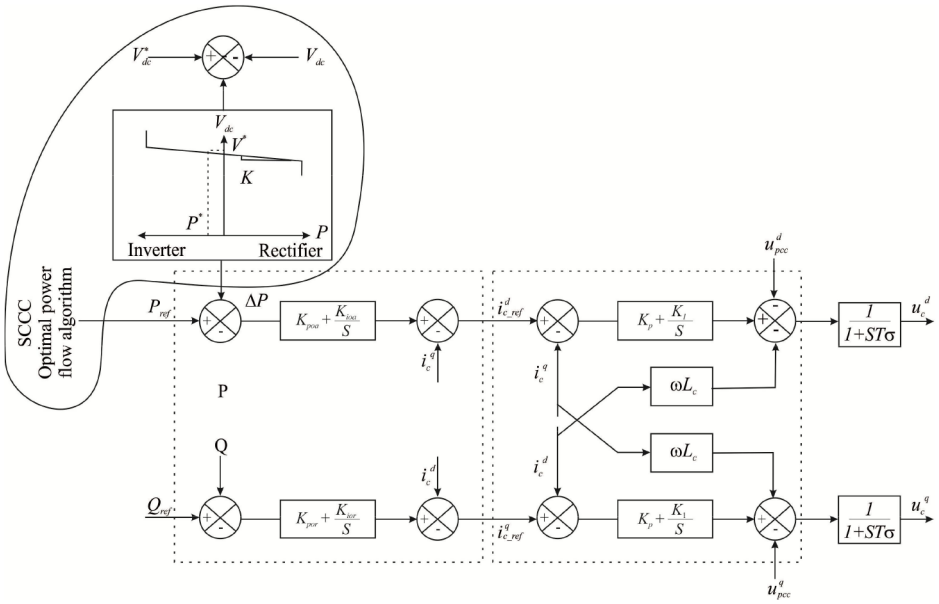

Figure 2. Control scheme of the grid side converter.

AC/DC lines connected to a wind farm. Obviously, the power pooled into the DC system can be injected into the AC system at a number of AC buses, and the shares of power among the different inverters depend on droop setting.

3. Power flow of VSC-MTDC

In its most general format, AC/DC sequential load flow analysis was well documented in [8]. The conventional Newton–Raphson AC load flow algorithm was modified to include the DC subsystem. Power fed into the DC grid from the AC system was modeled as load. Power pumped into the AC system from the DC grid was modeled as negative load from the AC load flow perspective. Though there is no reactive power flow through the DC link, the converters consume reactive power, which is again unknown prior to load flow. Reactive power flow through the converter transformer is governed by the voltage magnitudes and voltage angles of the converter AC bus and the terminal AC bus. The state variables are the magnitude and angle of AC bus voltages, DC bus voltages, and magnitude and angle of converter AC bus voltage. The AC load flow, DC load flow, and DC slack bus iterations are sequentially carried out to satisfy the three sets of mismatch equations.

3.1. Power flow of VSC MTDC with droop control

Generally, the buses in the DC link are classified as P-controlled buses, voltage-regulated buses, voltage margin-regulated buses, and droop-controlled buses. P-controlled buses are the rectifier bus, where P is frozen and voltage can vary. The voltage-regulated bus is commonly the slack bus, where V_{dc} is frozen and P can change. Voltage margin-regulated buses are inverter buses or back-up slack buses. Most commonly, the overrated inverter bus in the system serves as the DC slack bus. However, loss of this converter leads to the collapse of the entire DC grid. Thus, the idea of back-up slack buses with voltage margin control emerged. Nevertheless, the most versatile one is the droop control of the DC system, where more than one inverter bus serves the power balance within the DC system. It tries to control the power in and around the reference value and also contributes to power balancing while maintaining the DC system voltage profile in accordance with the voltage ratings.

The effect of droop control action is shown to be the power-sharing within the DC grid by regulating the DC voltages. Droop control essentially modulates p.u. change in power flow setting/p.u. change in DC voltage of droop-controlled DC buses. The DC bus voltage regulation is distributed among the droop-controlled buses in the DC grid. Unlike the slack bus in the AC system, DC voltages of all the droop-regulated buses are taken as a state variable. The regulation of the mean voltage of the DC link can be accommodated by considering an additional mismatch equation.

Power flow control within the DC grid through voltage droop is similar to that of frequency droop in the AC grid. In the case of the AC system, the lines flows are governed by angle difference, whereas in a meshed DC system the line flows are governed by DC voltage differences. The power imbalance in the DC subsystem is compensated by the slack bus, which demands a higher rating of DC slack bus. Instead, the responsibility is distributed among multiple converters. This prevents the overrating of the slack converter and thus reduces the cost of the DC subsystem.

The droop control should essentially include the currents and voltage limits. Basic V-P droop characteristics are shown in Figure 2 and implemented in OPF formulation. The power flows within the DC system are modulated by DC droop settings. DC buses are categorized into two types, droop control buses and power control buses. The power is modulated around a reference value by the droop factors:

$$P_{dc_n} = P_{dc_{nref}} + D_n(V_{dc_n} - V_{dc_{n,o}}) \tag{1}$$

where D_n is the voltage droop defined as $\frac{\Delta P_{dc}}{\Delta V_{dc}}$ in this paper, for the nth bus. The P mismatch equation for the droop-controlled bus is given by:

$$\Delta P_{dc_n} = V_{dc_n} \sum_{\substack{j=1 \\ j \neq N}}^{N} Y_{dc_{nj}} \left(V_{dc_n} - V_{dc_j}\right) - P_{dc_{nref}} + D_n \left(V_{dc_n} - V_{dc_{nref}}\right) \tag{2}$$

The power reference set point of droop-controlled buses is initialized as:

$$P_{dc_{kref}} = \text{Net power pooled by all the } WFSC \times \frac{\text{rating of } k^{th}\, GSC}{\text{sum of the rating of all } GSC} \tag{3}$$

The power balance equation in the DC system is given as:

$$\sum P_{WFSC} = \sum P_{GSC} + P_{net\_loss} \tag{4}$$

3.2. Droop control strategy 1

In this droop control strategy, the number of state variables is the same as the number of DC buses. The responsibility of voltage regulation is divided among n number of DC buses. The DC buses are categorized into two different types: droop-controlled and P-controlled buses. The GSC buses are assigned for droop control where P_{ref} is modulated. WFSCs are P-controlled where P is specified.

The specified parameters are:

$$P_{spec} = [D_1\, D_2 D_3 \ldots D_n\, P_{dc1}\, P_{dc2}\, P_{dc3} \ldots P_{dcm}] \tag{5}$$

where:

P_{spec} - Specified parameters

n - Number of droop-controlled buses

m - Number of injection-controlled buses

P_{dc} - Specified power injection at mth P-controlled bus

D - Specified droop setting at nth droop-controlled bus

The set of state variables is given by:

$$X = [V_{dc1} V_{dc2} V_{dc3} V_{dcn} V_{dc(n+1)} \dots V_{dc(n+m)}] \tag{6}$$

3.3. Droop control strategy 2

In this droop control strategy [7], the number of state variables is the number of DC buses plus one. The responsibility of voltage regulation is divided among all the DC buses. The set of state variables is given by:

$$X = [V_{dc1} V_{dc2} V_{dc3} V_{dcn} V_{dc(n+1)} \dots V_{dc(n+m)} V_{ave}] \tag{7}$$

$V_{ave}-$ Average DC voltage of all the DC buses

One additional mismatch equation is added to the existing set, given by:

$$V_{ave} - \frac{1}{n} \sum_{i=1}^{n+m} V_i = 0 \tag{8}$$

The Jacobian entries corresponding to this mismatch equation are computed by:

$$\frac{\partial}{\partial V_i} \left(V_{ave} - \frac{1}{n} \sum_{i=1}^{n+m} V_i \right) = -\frac{1}{n} \tag{9}$$

$$\frac{\partial}{\partial V_{ave}} \left(V_{ave} - \frac{1}{n} \sum_{i=1}^{n+m} V_i \right) = 1 \tag{10}$$

The AC load flow, the DC load flow with droop implementation, and the DC slack bus iterations [8] are carried out sequentially, using the Newton–Raphson method.

4. Implementation of VSC-MTDC OPF

OPF is the common tool employed to obtain optimal solutions in power system operation. This section presents the OPF model with droop settings in the GSC bus and injection control in the WFSC bus as optimization parameters. The optimization algorithm presented in this paper incorporates three different objective function formulations. The first formulation targets the minimization of total losses in the AC/DC system. The second objective function targets the enhancement of voltage regulation in the AC and DC buses. The third aims at optimizing the loadings in the AC and DC lines. The analysis in this work is based on power-based droop.

$$\min F = \zeta_1 f_1 + \zeta_2 f_2 + \zeta_3 f_3 \tag{11}$$

where $\zeta_1 \zeta_2 \zeta_3$ are adaptive weighing factors.

4.1. Objective function 1

$$f_1 = P_{loss} = P_{acloss} + P_{dcloss} + P_{vscloss} \tag{12}$$

Losses are computed as given in [7].

4.2. Objective function 2

Minimization of steady state voltage deviations is assigned more weighting factor during ride-through conditions.

$$F2 = \sum_{i=1}^{n} (\Delta V_i)^2 \tag{13}$$

4.3. Objective function 3

Objective function 3 aims at optimizing the share of power penetration in the AC and DC systems. During high wind season, optimizing the flows to maximize the power evacuation capability of the AC/DC system is more significant than minimizing the losses and the steady state voltage deviations. The objective function aims at utilizing the AC and DC transmission infrastructure to the maximum, rather than blocking the wind power in high wind seasons.

$$f_3 = \sum_{i=1}^{ac\,lines} (S_{i\_rated} - S_{i\_flow}) - \sum_{i=1}^{ac\,lines} (P_{i\_rated} - P_{i\_flow}) \tag{14}$$

Optimization parameters: $(D_1 D_2 \ldots D_n \beta_1 \beta_2 \beta_3, \ldots\ldots\ldots, \beta_n)$

D_i - Droop setting of ith GSC DC bus

β_i - % share of power penetration at ith bus into DC lines connected to ith bus

$\beta = W_i \times$ PPDC/100 - Share of power penetration at ith bus into DC lines connected to ith bus in MW

W_i - Wind power penetration at ith bus

Operating constraints, AC and DC bus voltage limits, AC and DC line transmission capacity limits, active and reactive power limits of the converter transformer, and operating constraints of converters are considered conventionally, as given in [14,15]. Figure 3 illustrates the proposed OPF algorithm. The weighing factors are modified adaptively according to the wind power penetrations and frequency of the AC grid. All mismatch equations in the mixed AC/DC load flow are imposed as equality constraints.

5. Results and discussion

5.1. Description of study system 1

The 3-machine 9-bus WSCC system is modified to a 12-bus system with wind penetrations at buses 10, 11, and 12. The AC and DC buses are interconnected by converters at 5 locations. The wind farm side substations are located at buses 10, 11, and 12 and a DC serial connected subsystem is formed by connecting DC buses 1, 2, 3, 4, and 5, as shown in Figures 4 and 5. The power pooled into the WFSCs is evacuated through grid side converters GSC 1 and 2, shown in Figures 4 and 5, which are connected to the AC system at buses 5 and 6. No loads are considered at buses 10, 11, and 12.

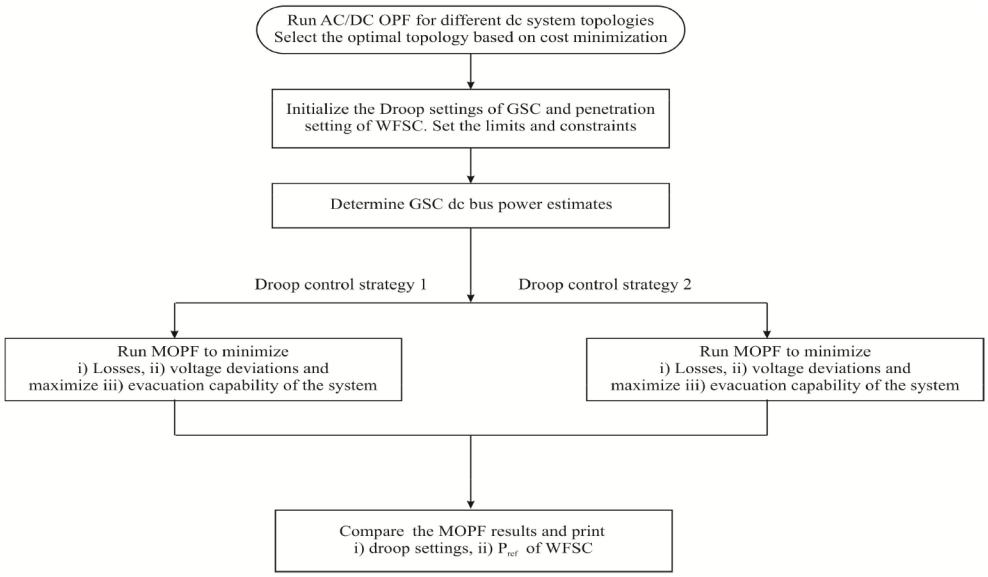

Figure 3. Flow chart of the MOPF algorithm.

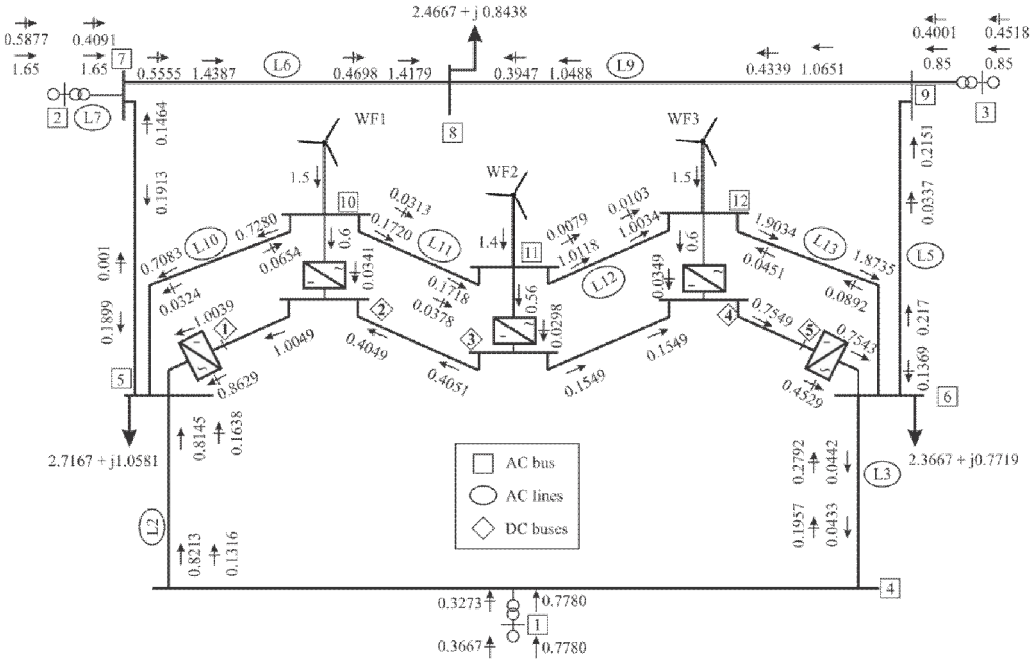

Figure 4. Power flow diagram for 40% wind power penetration through the DC system.

It is assumed that whatever the type of wind turbine generator (WTG), the penetration into the AC/DC system is only the real power and the reactive power demand of the WTG is locally met. A wind power penetration scenario (WPPS) is considered as shown in Table 1. The types of DC buses and converters are given in Table 2. The ratings of the system are as shown in Table 3. Power injections are specified for all the rectifier buses, i.e. WFSC buses, and one inverter bus, i.e. the GSC2 bus. DC voltage is specified for the DC slack bus, i.e. GSC1, which has the highest rating (300 MVA).

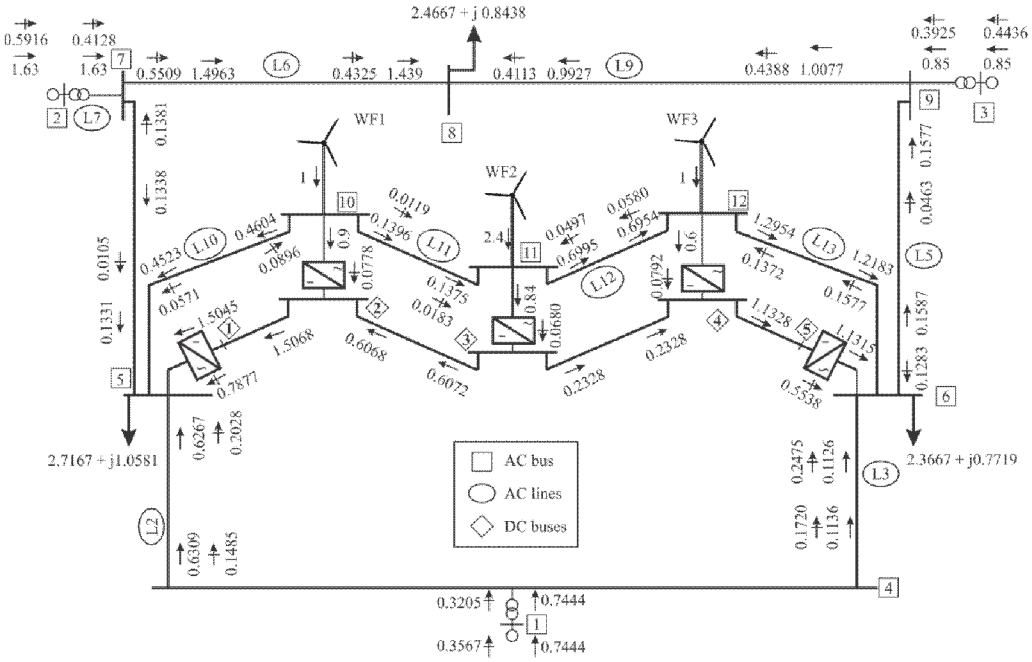

Figure 5. Power flow diagram for 60% wind power penetration through the DC system.

Table 1. Wind power penetration scenario.

Wind power	Wind power	Wind power	Total wind
generation at WF1	generation at WF2	generation at WF3	power
150 MW	140 MW	150 MW	440 MW

Table 2. Type of DC converter.

DC converter	Type	Control
1	Gide side converter (GSC1)	DC slack
2	Wide farm side converter (WFSC1)	P control
3	Wide farm side converter (WFSC2)	P control
4	Wide farm side converter (WFSC3)	P control
5	Gide side converter (GSC2)	P control

The active power reference settings of GSC1 and GSC2 are governed by the ratings of the GSC. The power that is pooled by the WFSCs into the DC system is evacuated in a fixed proportion, depending on the rating of the converters.

$$P_{ref}of\,GSC\,1 = \frac{WF1 + WF2 + WF3}{\text{Rating of}\,GSC1 + \text{Rating of}\,GSC2} \times \text{Rating of}\,GSC\,1 \tag{15}$$

$$P_{ref}of\,GSC\,2 = \frac{WF1 + WF2 + WF3}{\text{Rating of}\,GSC1 + \text{Rating of GSC2}} \times \text{Rating of GSC}\,2 \tag{16}$$

With the rating of GSC1 being 300 MVA and that of GSC2 being 220 MVA, as shown in Table 3, the ratio works out to be 57.69:42.31.

Table 3. Ratings of the extended 9 bus system.

DC system	Rating in MVA
Wind farm side converter 1	150
Wind farm side converter 2	250
Wind farm side converter 3	150
Grid side converter 1	300
Grid side converter 2	220
DC line 1	300
DC line 2	150
DC line 3	150
DC line 4	225

5.2. Load flow analysis for modified 3-machine 9-bus system

In order to clearly identify the need for optimizing the droop settings and injection settings, constraints are not imposed on variables. It is assumed that the wind farm injects power at unity power factor (p.f), maintained by local compensators. In order to analyze the effect of routing the power in AC and DC lines in different proportions, two different percentage penetrations through DC lines (PPDC) are considered.

Case 1: Of the total power generated by WG, 40% of power is scheduled to flow into the DC system and 60% of power is wheeled through AC lines.

Case 2: Of the total power generated by WG, 60% of power is scheduled to flow into the DC system and 40% of power is wheeled through AC lines.

The results of the load flow analysis are given in Table 4. Table 5 shows the comparison of losses and real power generation for two different PPDC values. It is observed that the AC losses are less for 60% PPDC when compared to 40% PPDC. Voltages at nodes 1, 2, and 3 are constant, since those nodes are PV buses where synchronous generators are located. The generator operates within the Q limits. Figures 4 and 5 show the power flows in the modified 3-machine 9-bus system for 40% and 60% PPDC.

Table 4. Load flow results of the modified 3-machine 9-bus system for different percentages of penetration through the DC system (PPDC).

Voltages in p.u.	Case 1	Case 2
V4	1.0206	1.0211
V5	1	1
V6	1	1
V7	0.9941	0.9939
V8	0.9442	0.9442
V9	1.0004	1.0008
V10	1.0253	1.0152
V11	1.0235	1.0138
V12	1.0151	1.0090
V_{DC1}	1	1
V_{DC2}	1.001004	1.001505
V_{DC3}	1.0014	1.0021
V_{DC4}	1.001254	1.001878
V_{DC5}	1.0005	1.0007

Table 5. Comparison of losses for different percentages of penetration through the DC system (PPDC).

	Case 1	Case 2
Total real power generation by SG in MW	325.8	322.44
Total reactive power generation by SG in MW	140.62	139.21
AC loss in MW	10.63	7.04
DC loss in MW	0.18	0.40
Converter loss in MW	0.21	0.28
Power flow into the DC system through WFSC1 in MW	60	90
Power flow into the DC system through WFSC2 in MW	56	84
Power flow into the DC system through WFSC3 in MW	60	90
Power evacuated by GSC1 in MW	100.39	150.45
Power evacuated by GSC2 in MW	75.43	113.15
% of power evacuated by GSC1	57.09	57.07
% of power evacuated by GSC2	42.90	42.98
Total wind power penetration through WFSC in MW	176	264
Total wind power evacuation through GSC in MW	175.82	263.60

The DC losses and converter losses are less when compared to the AC losses. Net Q generation by all SGs is 140.62 for 40% wind power penetration, which is high when compared to 139.21 for 60% penetration. The voltages at AC buses 10, 11, and 12 decrease as the percentage penetration into DC increases. The power injected by the GSCs into the AC system is represented by dummy generators in AC load flow. Thus, voltage at buses 5 and 6, where GSCs are connected, remains at 1 p.u. When PPDC is increased beyond 75%, the load flow solution diverges.

AC losses are 7.04 MW for 60% PPDC and 10.63 MW for 40% PPDC, whereas the voltage profile at bus 7 for 40% PPDC is better when compared to 60%. This is because the power injection into the DC system is modeled as load in the AC load flow. The power penetration from the WTG is modeled as negative load. As the PPDC is increased, it is as though loading is increased in AC buses 10, 11, and 12, since the flow into the DC grid is modeled as load in AC side. Flows into AC lines 10, 11, 12, and 13 change as the PPDC changes. It is the DC bus voltage differences that govern the power flow through the DC link; thus, they change accordingly, but are very close to 1 p.u., as shown in Table 4. A small change in voltage difference causes a large change in power flow.

It can be concluded that as the PPDC varies, losses, real and reactive power generation of SG in the system, and AC and DC voltages vary. It depends on the network, the wind power penetration, and the loads in the system. However, no generalized conclusion about whether it may increase or decrease as the PPDC increases/decreases can be reached based on the above results. From the above discussion it is evident that an optimization is required to optimize the injection settings and the share of power evacuated by the GSCs, which can be controlled by optimal droop settings.

5.3. Droop implementation in load flow analysis of 3-machine 9-bus system

Four different droop settings are considered for analysis, as shown in Table 6. Comparison of load flow results with different droop settings are shown in Tables 7 and 8. The share of power pumped into the DC system is held constant (i.e. the study is performed for 60% PPDC). The share of power evacuated by GSC1 and GSC2 changes as the droop settings are changed. The DC line flows, DC link voltages, and AC bus voltage profile also change with respect to droop coefficients.

Table 6. Droop-setting cases.

Droop	Case 1	Case 2	Case 3	Case 4
Droop 1(pertaining to GSC1)	0.008	0.005	0.001	0.008
Droop 2(pertaining to GSC2)	0.003	0.007	0.001	0.008

Table 7. Load flow results of modified 3-machine 9-bus system with different droop settings for 60% PPDC.

Case	Case 1	Case 2	Case 3	Case 4
V4	1.0212	1.0212	1.0205	1.0212
V5	1	1	1	1
V6	1	1	1	1
V7	0.9938	0.9938	0.9942	0.9939
V8	0.9442	0.9442	0.9442	0.9442
V9	1.0009	1.0009	1.0003	1.0009
V10	1.0157	1.0156	1.0132	1.0155
V11	1.0142	1.0141	1.0126	1.0140
V12	1.0092	1.0092	1.0083	1.0091
V_{DC1}	0.9991	0.9995	1.0004	0.9995
V_{DC2}	1.0008	1.0011	1.0015	1.0011
V_{DC3}	1.0015	1.0018	1.0017	1.0018
V_{DC4}	1.0014	1.0017	1.0011	1.0016
V_{DC5}	1.0003	1.0007	0.9996	1.0005

Table 8. Comparison of losses and real power generation with different droop settings for 60% PPDC.

Case	For 60 % PPDC			
	Case 1	Case 2	Case 3	Case 4
Total real power generation by SG in MW	322.4	322.4	322.97	328.41
Total reactive power generation by SG in MW	138.88	138.92	140.67	139.01
AC loss in MW	6.98	6.99	7.58	7.00
DC loss in MW	0.42	0.41	0.40	0.41
Converter loss in MW	0.28	0.28	0.28	0.28
Power evacuated by GSC1 in MW	161.6	160.04	113.03	156.95
Power evacuated by GSC2 in MW	101.98	103.54	150.57	106.64
% of power evacuated by GSC1	61.08	60.71	42.87	59.54
% of power evacuated by GSC2	38.69	39.28	57.12	40.45
Total wind power penetration through WFSC in MW	264	264	264	264
Total wind power evacuation through GSC in MW	263.58	263.59	263.6	263.59

The real and reactive power generation of the slack bus varies as the losses in the system vary. From the results, it can be concluded that the droop settings govern the flows in the DC lines. The impact on the AC system is to vary the losses and voltage profile. By comparing Tables 4 and 5 with Tables 7 and 8, it can be concluded that the impact of changing PPDC is stronger than that of changing the droops.

Since the buses to which the GSCs are connected are taken as PV buses by assuming dummy generators in AC load flow, the voltages at buses 5 and 6 remain at 1 p.u. Flows in the AC system vary due to changes in injections at buses 5 and 6, which causes variation in AC system losses, as shown in Table 8. The results reveal the need for optimization to minimize the losses and optimize the flows through the AC and DC lines.

5.4. Droop optimization results of modified 3-machine 9-bus system

Droop settings, injection settings, and DC bus reference voltage are considered as optimization parameters. Bounds on optimization parameters are given in Table 9. The results are given in Tables 10 and 11. Without optimization, the results presented in Tables 4 and 5 are compared to the results presented in Tables 10 and 11 and Figure 6. The total losses in the system are 11.02 and 7.72, as shown in Table 5, whereas when droop and injections are optimized, losses are reduced to 5.97, as shown in Table 11. Though there is an overall decrease in losses, the DC losses increase from 0.4 to 0.86 MW, and converter losses increase from 0.28 to 0.4 MW. The real power generation of the slack bus has been reduced, as shown in Table 11. The reactive power generation of all synchronous generators has been reduced and the voltage profile has improved for optimized droop and injection settings. The share of power evacuated by GSCs is no longer in fixed proportion. The share of GSCs is found to be 49:51, as seen in Table 11. As DC reference voltage can vary within bounds, neither losses nor the voltage profile are found to improve.

Table 9. Bounds on optimization variables.

DC system	Lower bound	Upper bound
Droop 1	0.0001	0.008
Droop 2	0.0001	0.008
DC bus voltage reference of GSCs	0.95	1.15
% penetration through DC link in all three WFSCs	0	1

Table 10. Load flow results with optimization.

V4	1.0212
V5	1
V6	1
V7	0.9938
V8	0.9442
V9	1.0009
V10	1.0156
V11	1.0141
V12	1.0092
V_{DC1}	1.0003
V_{DC2}	1.0022
V_{DC3}	1.0026
V_{DC4}	1.0017
V_{DC5}	0.9997

5.5. Description of study system 2

The system considered for testing the algorithm is part of an Indian utility grid. Wind power is abundant in South Tamil Nadu, Tirunelveli region. There is a need for strengthening the transmission infrastructure as wind farms appear faster. VSC-MTDC networks offer the advantage of enhancing the evacuation capability needed to keep in pace with capacity additions. The system consists of 156 buses and 44 dedicated wind farm substations. In the serial five-bus system shown in Figure 7, wind farms are located near buses 2, 3, and 4. The GSCs are located at buses 1 and 5. The ratings of all the WFSCs are 200 MVA, GSC1 is 250 MVA, and GSC2 is 350 MVA.

Table 11. Comparison of losses and real power generation with optimization.

Case	
Total real power generation by SG in MW	320.57
Total reactive power generation by SG in MW	138.72
AC loss in MW	4.71
DC loss in MW	0.86
Converter loss in MW	0.40
Power flow in to DC system through WFSC1 in MW	150
Power flow in to DC system through WFSC2 in MW	136.48
Power flow in to DC system through WFSC3 in MW	102.75
Power evacuated by GSC1 in MW	190.06
Power evacuated by GSC2 in MW	198.31
% DC penetration in DC bus 2	100
% DC penetration in DC bus 3	97.49
% DC penetration in DC bus 4	68.50
% of power evacuated by GSC1	49
% of power evacuated by GSC2	51
Droop 1	0.0014
Droop 2	0.001
Total wind power penetration through WFSC in MW	389.23
Total wind power evacuation through GSC in MW	388.37
Optimization function	0.0557

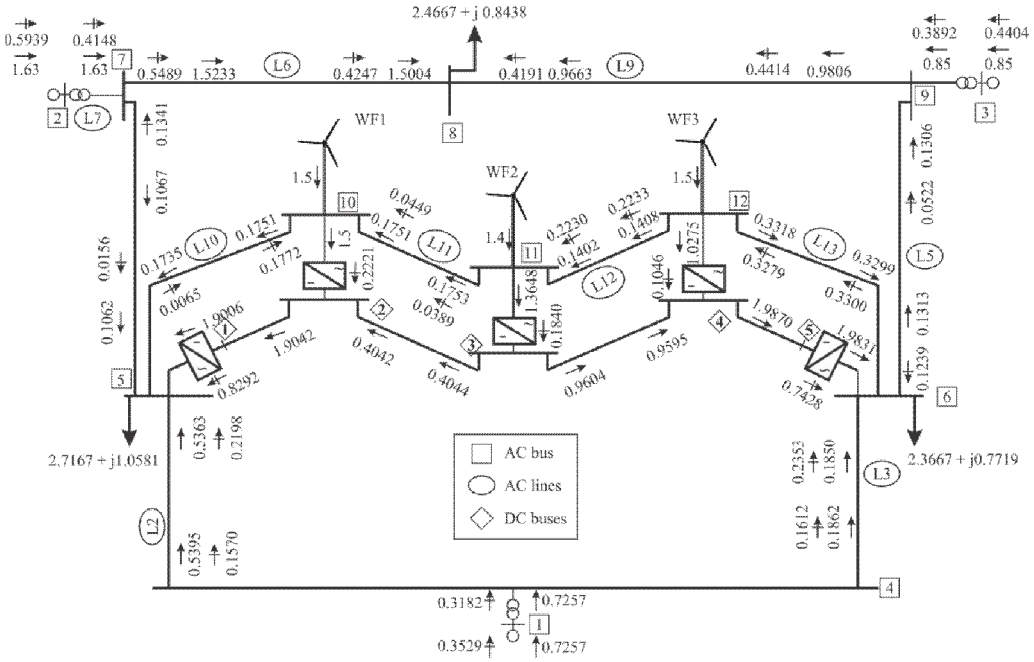

Figure 6. Power flow diagram for optimized injection and droop settings.

5.6. Selection of topology and rating of the subsystem

The technical feasibility of a backbone DC grid embedded in the existing Tirunelveli AC system is analyzed. Power is wheeled through 33-kV lines, pooled via 110-kV substations, and connected to the load center via a 400-kV link. During high wind penetrations, overloadings are observed in various 110-kV lines rated 90 MVA

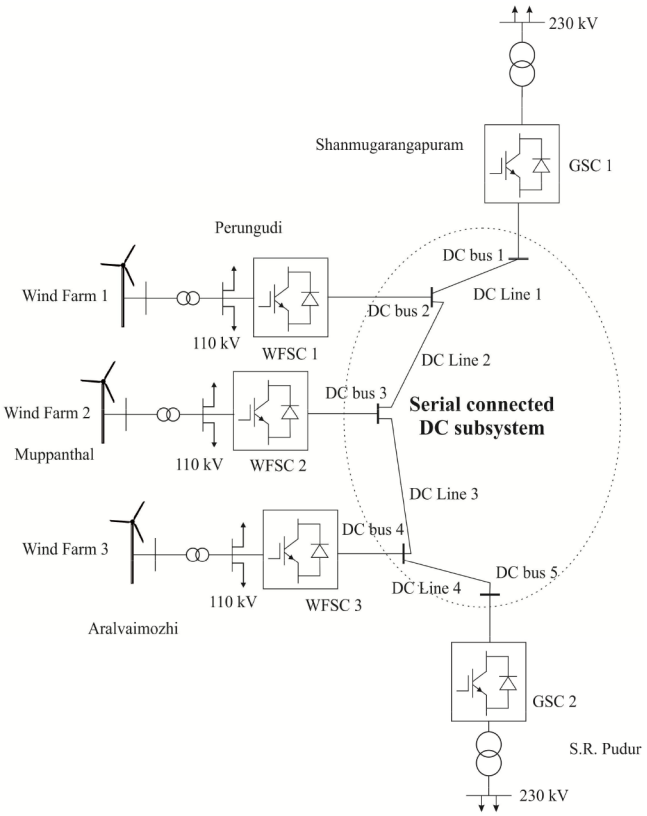

Figure 7. Configuration of the studied test system.

and 110/230 kV transformers. The impacts of different DC grid topologies, such as serial, radial, and mesh topologies for various congestion pockets, are investigated for high wind power penetrations. This is done as a preoptimization problem, as given in [14]. A serial topology of the meshed DC system is taken as the test system, as shown in Figure 7.

5.7. Droop optimization results of the Tirunelveli subsystem

The MOPF model discussed in Section 4 is applied to the test VSC-MTDC system. The transmission system is incrementally stressed by increasing wind power penetration in all three wind farms in steps of 5% around the base case. Ten different cases were considered for analyzing the validity of the proposed formulation, as given in Table 12.

Two different droop control strategies were considered for the OPF solution. The results reveal that from an optimization point of view the strategies are similar. It is observed that as the wind power penetration increases, as shown in Figure 8a, the droop of both of the GSCs increases, as shown in Figure 8b. When power pooled into the DC system increases, this is to be anticipated, since the MW/p.u. voltage has to increase in order to pump more power. DC bus penetrations are found to increase as the wind power penetration increases, as shown in Figures 8c and 8d. Figure 8e shows that the share of AC bus penetrations is less when compared to DC bus penetrations, as DC losses are less when compared to AC losses. Variations of losses are shown in Figure 8f. It is observed from Figure 8g that voltage at DC bus 5 decreases as wind power increases; this is because the difference between the voltages drives the power flow. The voltage of DC bus 1 increases by smaller magnitudes. The voltages of those DC buses connected to WFSC increase as penetration increases.

Table 12. MOPF solutions for different wind power penetrations.

Case	Wind farm output In p.u.			Share of power pumped into AC lines in p.u.			Power injection/drawl at D buses					Droop 1 MW/p.u. DC voltage	Droop 2 MW/p.u. DC voltage	DC line flows in p.u.			
	WF 1	WF 2	WF 3	AC bus 2	AC bus 3	AC bus 4	P_{dc1}	P_{dc2}	P_{dc3}	P_{dc4}	P_{dc5}			Line 1	Line 2	Line 3	Line 4
1	1.365	1.925	1.75	0.6921	0.7102	0.7335	134.33	0.6729	1.2148	1.0165	1.5128	0.00031	0.0002	1.3433	0.693	0.5192	1.5128
2	1.462	2.062	1.875	0.7031	0.7178	0.7374	149.79	0.7549	1.3447	1.1376	1.6841	0.00034	0.00026	1.4979	0.7666	0.5749	1.6841
3	1.56	2.2	2	0.7211	0.7292	0.7433	164.46	0.8389	1.4708	1.2567	1.8499	0.00041	0.00035	1.6446	0.8395	0.6275	1.8499
4	1.657	2.337	2.125	0.748	0.7465	0.752	178.09	0.9095	1.591	1.373	2.0082	0.00049	0.00047	1.7809	0.911	0.6756	2.0082
5	1.755	2.475	2.25	0.7588	0.7549	0.7583	181.94	0.9962	1.7209	1.4917	2.289	0.0006	0.00059	1.8194	0.8632	0.85	2.289
6	1.852	2.612	2.375	0.7879	0.769	0.7576	188.53	1.0646	1.8435	1.6174	2.5246	0.00072	0.00069	1.8853	0.863	0.9714	2.5246
7	1.95	2.75	2.5	0.8382	0.7931	0.7521	197.68	1.1118	1.9569	1.7479	2.7089	0.00084	0.00079	1.9768	0.9115	1.03	2.7089
8	2.047	2.887	2.625	0.8938	0.8213	0.745	206.05	1.1537	2.0662	1.88	2.8928	0.00097	0.00091	2.0605	0.9573	1.0974	2.8928
9	2.145	3.025	2.75	0.9537	0.8537	0.736	213.73	1.1913	2.1713	2.014	3.0763	0.00111	0.00109	2.1373	1.0005	1.158	3.0763
10	1.365	1.925	1.75	1.0177	0.8896	0.7253	220.81	1.2248	2.2729	2.1497	3.2593	0.00122	0.00118	2.2081	1.0415	1.2173	3.2593

Flows on 100 MVA base.

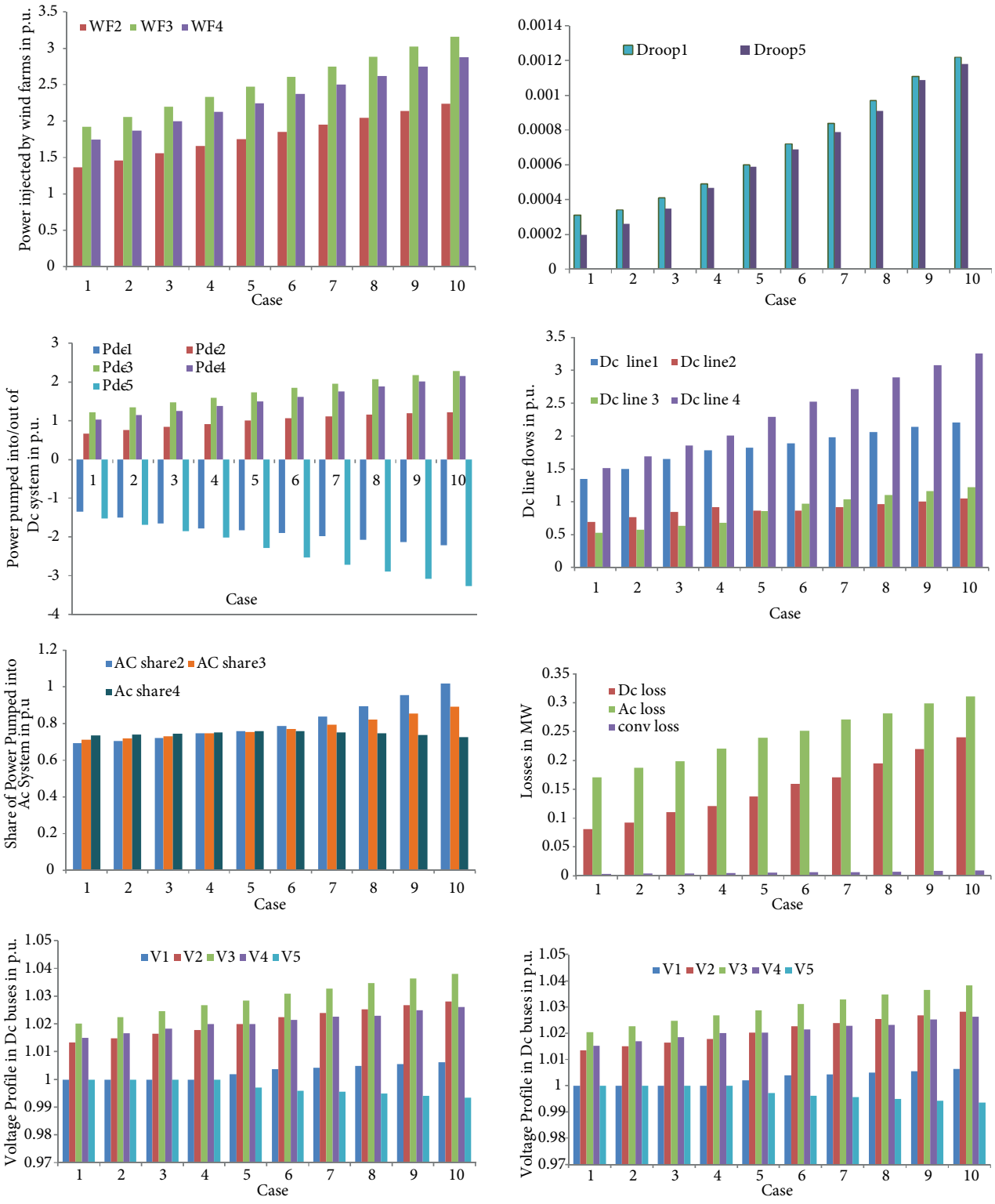

Figure 8. a) Wind power penetrations at AC buses 2, 3, and 4; b) droop settings of GSC; c) DC bus injection/drawl; d) DC line flows; e) share of power into the AC system at wind power penetrating buses; f) losses in the AC/DC system; g) voltages at DC buses; h) net penetration into the AC and DC systems.

In Table 12, the injection settings of WFSCs at DC buses 2, 3, and 4 are tabulated. Power pumped into WFSCs is evacuated through both GSCs in proportion to the rating of the converters. The power reference settings of the GSC are dictated by the rating of the converters and the power pooled into the DC link. The settings are modulated by droop factors computed by the optimal power flow algorithm, which is a part of the SCCC. The power evacuated by the GSC at DC buses 1 and 5 is shown in Table 12. As the wind power penetration increases, the percentage share of penetration into AC buses 2, 3, and 4 decreases, although actual flows in MW seem to increase, as shown in Table 12. Furthermore, if the wind power penetration is increased, the transmission line limits and droop limits are hit (not shown).

Optimizing the power evacuation capability along with losses and voltage deviations yields better results when compared to optimization losses alone. Optimizing losses alone is an optimistic result from a loss minimization point of view. However, adding maximization of evacuation capability in the objective function yields better results, because optimizing both the AC and DC line loadings gains more significance, especially in high wind seasons at the cost of a small increase in losses. When wind power is abundant, more emphasis on increasing the evacuation capability of the AC/DC system gains more significance, rather than minimizing the losses.

A tradeoff is achieved between minimizing losses and maximizing power evacuation capability, depending on wind fluctuations and the frequency of the AC grid. The objectives are better achieved when the share of the AC subsystem (or the share of the DC subsystem) at each and every wind power penetration bus is taken as an optimization parameter, along with droop settings at GSCs. Of the total wind power penetration, the share of the AC system is found to be less when compared to the DC system, as shown in Figure 8h.

6. Conclusion

In this paper, a modified OPF model incorporating a detailed VSC-MTDC with droop regulation is proposed. This model is used as a calculation engine to determine the droop settings and the power injection settings at GSCs and WFSCs, respectively. Wind power penetrations are routed into AC lines and DC lines in different proportions. These proportions are determined by optimizing the flows in various AC/DC lines connected to a wind farm. The power pooled into the DC system is injected into the AC system at droop-controlled inverter buses. The share of power between the different inverters is determined by the droop setting, computed using the proposed OPF algorithm. The proposed MOPF algorithm is tested on a preoptimized serial-connected DC system embedded in a practical utility system. The losses in the AC/DC system and steady state voltage deviations are minimized, and the power evacuation capability of the AC/DC system is maximized. It is observed that at the cost of a small increase in losses, flows in the AC and DC lines are optimized to enhance the power evacuation capability of the AC/DC system.

Acknowledgments

This work is the outcome of project funded by the National Institute of Wind Energy, Ministry of New and Renewable Energy, Government of India (Project No: RD-RD-192-10). The authors sincerely thank the Tamil Nadu Electricity Board for its support.

Nomenclature

GSC	Grid side converter
PCC	Point of common coupling
PPDC	Percentage penetration into DC link

VSC-MTDC	Voltage source converter-based high voltage direct current
SCCC	Slow centralized coordinated controller
SCR	Short circuit ratio
WFSC	Wind farm side converter
WPPS	Wind power penetrating scenario
WTG	Wind turbine generator

References

[1] Flourentzou N, Agelidis VG, Demetriades GD. VSC-based HVDC power transmission systems: an overview. IEEE T Power Electr 2009; 24: 592-602.

[2] Lu W, Ooi BT. Optimal acquisition and aggregation of offshore wind power by multiterminal voltage source HVDC. IEEE T Power Deliver 2003; 18: 201-206.

[3] de Alegria IM, Martin JL, Kortabarria I, Andreu J, Ereno PI. Transmission alternatives for offshore electrical power. Renew Sust Energ Rev 2009; 13: 1027-1038.

[4] Zhang L, Harnefors L, Nee HP. Interconnection of two very weak AC systems by VSC-HVDC links using power-synchronization control. IEEE T Power Syst 2011; 26: 344-355.

[5] Hertem DV, Ghandhari M. Multi-terminal VSC HVDC for the European supergrid: obstacles. Renew Sust Energ Rev 2010; 14: 3156-3163.

[6] Beerten J, Hertem DV, Belmans R. VSC MTDC systems with a distributed DC voltage control – a power flow approach. In: IEEE 2011 PowerTech; 19–23 June 2011; Trondheim, Norway. New York, NY, USA: IEEE. pp. 1-6.

[7] Wang W, Barnes M. Power flow algorithms for multi-terminal VSC-HVDC with droop control. IEEE T Power Syst 2014; 29: 1721-1730.

[8] Beerten J, Cole S, Belmans R. Generalized steady-state VSC MTDC model for sequential AC/DC power flow algorithms. IEEE T Power Syst 2012; 27: 821-829.

[9] Prieto-Araujo E, Bianchi FD, Junyent-Ferre A, Gomis-Bellmunt O. Methodology for droop control dynamic analysis of multiterminal VSC-HVDC grids for offshore wind farms. IEEE T Power Deliver 2011; 26: 2476-2485.

[10] Aragues-Penalba M, Egea-Alvarez A, Gomis-Bellmunt O, Sumper A. Optimum voltage control for loss minimization in HVDC multi-terminal transmission systems for large offshore wind farms. Electr Pow Syst Res 2012; 89: 54-63.

[11] Pinto RT, Bauer P, Rodrigues SF, Wiggelinkhuizen EJ, Pierik J, Ferreira B. A novel distributed direct-voltage control strategy for grid integration of offshore wind energy systems through MTDC network. IEEE T Ind Electron 2013; 60: 2429-2441.

[12] Haileselassie TM, Uhlen K. Impact of DC line voltage drops on power flow of MTDC using droop control. IEEE T Power Syst 2012; 27: 1441-1449.

[13] Eriksson R, Beerten J, Ghandhari M, Belmans R. Optimizing DC voltage droop settings for AC/DC system interaction. IEEE T Power Deliver 2014; 29: 4588-4597.

[14] Feng W, Tuan LA, Tjernberg LB, Mannikoff A, Bergman A. A new approach for benefit evaluation of multiterminal VSC-HVDC using a proposed mixed AC/DC optimal power flow. IEEE T Power Deliver 2014; 29: 4588-4597.

[15] Cao J, Du W, Wang HF, Bu SQ. Minimization of transmission loss in meshed AC/DC grids with VSC-MTDC networks. IEEE T Power Syst 2013; 28: 3047-3055.

[16] Beerten J, Belmans R. Analysis of power sharing and voltage deviations in droop-controlled DC grids. IEEE T Power Syst 2013; 28: 4588-4597.

[17] Bidadfar A, Abedi M, Karrari M, Gharehpetian GB, Tavana SN. Passive AC network supplying the integration of CCC-HVDC and VSC-HVDC systems. Turk J Elec Eng & Comp Sci 2014; 22: 353-362.